

# Piece-wise linear dynamic analysis of serpentine belt drives with a one-way clutch

F Zhu and R G Parker\*

Department of Mechanical Engineering, The Ohio State University, Scott Laboratory, Ohio, USA

The manuscript was received on 4 January 2007 and was accepted after revision for publication on 23 August 2007.

DOI: 10.1243/09544062JMES578

**Abstract:** A prototypical three-pulley serpentine belt drive with belt bending stiffness is extended to include a one-way clutch in order to understand the non-linear dynamics of the system with the one-way clutch performance. The clutch is modelled based on the relative velocity of the driven pulley and its accessory. The clutch locks (engages) the pulley and accessory for zero relative velocity and produces a positive inner clutch torque. Zero clutch torque initiates clutch disengagement, allowing unequal velocities of the two components. This model leads to a piece-wise linear system. The transition matrix is used to evaluate the system response in discrete time series for the two linear configurations, saving significant computational time. The system dynamics including response and dynamic tension drop are examined for varying excitation frequencies, inertia ratio of the pulley and accessory, and external load. The investigation of vibration reduction because of the single-direction power transmission of the clutch provides design guidelines in practice.

**Keywords:** one-way clutch, overrunning pulley, tensioner, serpentine belt drive, belt vibration, belt-pulley system, non-linear dynamics, piece-wise (piecewise) linear system

## 1 INTRODUCTION

Serpentine belts power automotive front-end accessory drives (FEADs), where a single belt transmits power from the crankshaft to a variety of accessories. The linear/non-linear mechanics of this system are examined in a group of studies [1–9]. A spring-like belt model is considered in references [1] to [3] to focus on the pulley rotational vibration. In references [4] to [7], the theory of string-like moving media is adopted for the serpentine belt to examine the belt transverse vibration as well as the pulley rotational vibration. Beikmann *et al.* [5] develop a prototypical three-pulley system involving a driving pulley, a driven pulley, and a tensioner (Fig. 1). The tensioner consists of a rigid arm rotating around its pivot and

a pulley pinned at the other end of the arm. It maintains the belt tension during operation.

Adopting the prototypical three-pulley system, Kong and Parker [8] establish a hybrid continuum–discrete model considering belt bending stiffness. The steady-state equilibrium solutions are obtained. Unlike the string-like belt model, non-trivial span equilibrium curvature occurs, which induces coupling of belt transverse vibration and pulley rotational vibration. In their subsequent work [9], the span–pulley coupling, which does not occur with string models, is investigated through the modal analysis of the system. This coupling is observed in experiments [6].

One-way clutches are used in mechanical systems such as the air turbine starters of a jet engine [10], helicopter main rotors, and certain pulleys in FEADs [11–15]. The clutch disengages when the driven or power-absorbing member (e.g. an automotive accessory) overruns the driving member (e.g. the pulley); in contrast, the two members are either locked together or connected through a spring-like

\*Corresponding author: Department of Mechanical Engineering, The Ohio State University, Scott Laboratory, 201 W. 19th Avenue, Columbus, OH 43210-1142, USA. email: parker.242@osu.edu

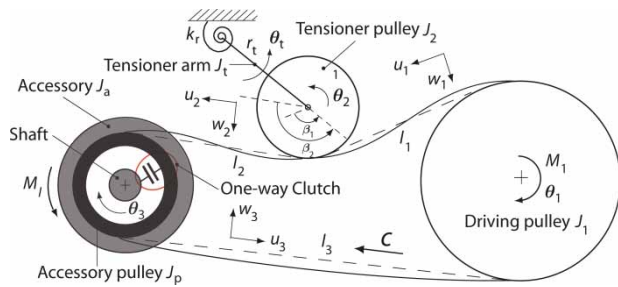


**Fig. 1** Three-pulley system with a one-way clutch integrated in the driven pulley and its associated accessory. The tildes on the physical quantities have been dropped for simplicity

element when their velocities are the same. Engagement ensures power transmission, whereas disengagement is for decoupling the two members to reduce or eliminate the influence from the heavy driven member during its overrunning. Such influence includes system vibration, belt flapping, belt wear, and chirp noise from belt–pulley friction. In this study, the application of a one-way clutch in serpentine drives is considered.

Vernay *et al.* [10] experimentally study the transient behaviour of sprag-type overrunning clutches to demonstrate the sliding effects during clutch engagement. King and Monahan [11] introduce the structure of a wrap-spring type overrunning pulley and address its design and installation. Solfrank and Kelm [12] make a comprehensive simulation of the accessory drive operation. The model of the one-way clutch consists of a velocity-dependent damping and a parallel spring with non-linear stiffness for torque transmission from the pulley to the accessory. The clutch intervenes only when the velocity of the accessory is lower than that of the pulley. Leamy and Wasfy [15] develop a dynamic finite-element model to determine the transient and steady-state response of a pulley–belt-drive system. To demonstrate the utility of the method, a one-way clutch that is modelled using a proportional torque law is incorporated into the driven pulley of the system, and its transient response is simulated.

The aforementioned literature, however, does not address the detailed dynamics of the one-way clutch. To examine its non-linear dynamics, Zhu and Parker [13, 16] model a two-pulley–belt system with a one-way clutch integrated between the driven pulley and its accessory. The clutch is a piecewise linear spring with discontinuous stiffness that engages only for positive relative displacement of its connected components. Through the simulation of its alternate engagement and disengagement behaviour, a classical softening non-linearity is identified. The clutch separates the pulley and accessory into two degrees of freedom (DOFs) and functions like a

vibration absorber to reduce vibration. Mockensturm and Balaji [14] present a piece-wise linear analytical method to investigate the dynamic behaviour of one-way clutches that are modelled on the basis of the relative velocity of the pulley and accessory shaft. The clutch operation leads to an increase in power transmission and a decrease in belt tension fluctuation.

In the above studies, only the pulley rotational vibration is considered. To more realistically examine the dynamics of serpentine belt drives with a one-way clutch, the present work adopts the typical three-pulley–belt system (Fig. 1) and employs the hybrid continuum–discrete model in references [8] and [9] that incorporates belt bending stiffness and exhibits belt–pulley coupling. Integrated between the driven pulley and its accessory, the one-way clutch separates and locks the motions of the two components during disengagement and engagement, respectively. For this piece-wise linear system, in each linear configuration, the analytical solutions are evaluated in discrete time series through the transition matrix [17]. The transition time instants are sought using two criteria, i.e. zero relative velocity and zero clutch torque. The solutions are confirmed by numerical integration. To give practical design advice, the impact of the one-way clutch on the system dynamics is investigated across a range of excitation frequencies, inertia ratio of the pulley and accessory, and external load. A reduction in the dynamic tension of the belt is examined.

## 2 SYSTEM MODEL

Figure 1 shows a typical three-pulley–belt system. The belt travels at a constant speed  $c$  to transmit power from the driving pulley to the driven (accessory) pulley. The tensioner arm is coil-spring loaded with spring stiffness  $k_r$ . An excitation torque  $\tilde{M}_l$  is applied to the driving pulley, and the accessory is subjected to a constant external torque  $\tilde{M}_c$ .

A relative velocity-dependent one-way clutch is installed between the driven pulley and the accessory drawing power from the belt drive. This clutch model applies to sprag-type, roller-type, or wrap-spring type one-way clutches. Consider first the disengaged clutch, where the velocity of the pulley  $\dot{\theta}_p$  is less than that of the accessory  $\dot{\theta}_a$ . When the relative velocity approaches zero, the pulley and accessory lock together, i.e. the clutch engages. During engagement, the pulley and accessory are constrained to move together by an inner clutch torque  $\tilde{M}_c$ . In this case, the pulley with inertia  $J_p$  and the accessory with inertia  $J_a$  are combined as one body with inertia  $J_0 = J_a + J_p$ . When the clutch torque reduces from positive to zero, the pulley and accessory disengage. The

mathematical expressions for the engagement and disengagement statuses of the clutch and their switching criteria are listed in Table 1. This piece-wise linear system behaves linearly in both the engagement and disengagement configurations.

By employing Hamilton’s principle, Kong and Parker [8] derive non-linear equations of motion of the three-pulley–belt system, where the belt is modelled as a moving flexural beam and the departure and end-points of the three belt spans are the same as those for the straight belt. The inclusion of finite belt bending stiffness causes non-trivial steady-state span curvature that determines the degree of coupling between the pulley and belt behaviour, in contrast to decoupled belt–pulley motion based on straight steady-state curvature in a string-like belt model. They then linearize the equations about the non-trivial equilibria and investigate the belt–pulley coupling in free vibration analysis [9].

In the present system, the linearized dimensionless governing equations in the engaged configuration are similar to those in reference [9] and are written in the extended operator form

$$\mathbf{M}\ddot{\mathbf{Y}} + \mathbf{G}\dot{\mathbf{Y}} + \mathbf{K}\mathbf{Y} = \mathbf{F} \tag{1}$$

where  $\mathbf{Y} = \{y_1, y_2, y_3, \theta_1, \theta_2, \theta_3, \theta_t\}^T$  collects the continuum belt span and discrete pulley and tensioner rotations into an extended variable.  $\theta_i$  and  $\theta_t$  denote the rotations of the pulleys and tensioner arm about their equilibria.  $\theta_3$  refers to the rotation of the accessory–pulley when engaged, i.e.  $\theta_3 = \theta_p$ . Note that the rotation of the accessory  $\theta_a$  involves rigid body motion if disengagement occurs during a cycle.  $y_i$  is related to the transverse displacement of each span  $w_i$  as

$$\begin{aligned} y_1 &= w_1 - \frac{r_t}{l_1} x_1 \theta_t \cos \beta_1 \\ y_2 &= w_2 + \frac{r_t}{l_2} (x_2 - 1) \theta_t \cos \beta_2 \\ y_3 &= w_3 \end{aligned} \tag{2}$$

where  $x_{1,2} \in [0, 1]$  the spatial variable along each span,  $r_t$  the length of the tensioner arm, and  $l_i$  the span lengths. The  $y_i$  satisfy trivial boundary conditions as those of a pinned beam. The differential

**Table 1** Engagement and disengagement statuses of the clutch and their switching criteria

	Status	Switching criterion
Engagement	$\dot{\theta}_a = \dot{\theta}_p, M_c > 0$	$M_c = 0$
Disengagement	$\dot{\theta}_p < \dot{\theta}_a, M_c = 0$	$\dot{\theta}_a = \dot{\theta}_p$

operators  $\mathbf{M}$  and  $\mathbf{K}$  are self-adjoint and  $\mathbf{G}$  is skew-self-adjoint, with an appropriate inner product defined in reference [9].  $\mathbf{F}$  is a vector composed of the accessory loads as

$$\mathbf{F} = \left\{ 0, 0, 0, \frac{r_1}{r_t} M_1, 0, -\frac{r_3}{r_t} M_l, 0 \right\}^T \tag{3}$$

Following the non-dimensionalization in reference [9], the dimensionless quantities are

$$\begin{aligned} x_i &= \frac{\tilde{x}_i}{l_i}, & w_i &= \frac{\tilde{w}_i}{l_i}, & l &= \frac{l_1 + l_2 + l_3}{3} \\ t &= \tilde{t} \sqrt{\frac{P_0}{\rho l^2}}, & \varepsilon^2 &= \frac{EI}{P_0 l^2}, & s &= c \sqrt{\frac{\rho}{P_0}} \\ k_s &= \frac{k_r}{P_0 r_t}, & \eta &= \frac{EA}{P_0}, & m_i &= \frac{J_i}{\rho r_i l^2} \\ m_t &= \frac{J_t}{\rho r_t l^2}, & m_a &= \frac{J_a}{\rho r_3 l^2}, & m_p &= \frac{J_p}{\rho r_3 l^2} \\ M_1 &= \frac{\tilde{M}_1}{P_0 r_1}, & M_l &= \frac{\tilde{M}_l}{P_0 r_3}, & M_c &= \frac{\tilde{M}_c}{P_0 r_3} \end{aligned} \tag{4}$$

where the tilde denotes physical quantities. For the clutch engagement configuration,  $m_3 = m_0$ . Considering the accessory as a free body separated from the pulley, its equation of motion is

$$m_a \ddot{\theta}_a + c_g \dot{\theta}_a = M_c - M_l \tag{5}$$

where  $M_c > 0$  enforces engagement and  $c_g$  is the accessory damping.

Equation (1) also applies to the clutch disengagement configuration, but only the pulley inertia is active, i.e.  $m_3 = m_p$ . In this case,  $\theta_3$  in equation (1) represents the accessory–pulley rotation only, i.e.  $\theta_3 = \theta_p$ , and  $\mathbf{F} = 0$ . The accessory rotates separately from the pulley and carries the load alone. It satisfies equation (5) but with zero clutch torque  $M_c = 0$ .

Similar to reference [9], a Galerkin discretization is applied to the hybrid discrete–continuous system (1). The extended variable  $\mathbf{Y}$  is expanded in a series of basis function as

$$\mathbf{Y} = \sum_{k=1}^p a_k(t) \boldsymbol{\psi}_k(x) + \sum_{k=1}^3 \theta_k(t) \boldsymbol{\psi}_{p+k}(x) + \theta_t(t) \boldsymbol{\psi}_t(x) \tag{6}$$

where  $p = N_1 + N_2 + N_3$  and  $N_i$  is the number of basis function for the  $i$ th span.  $\boldsymbol{\psi}_i$  are global comparison functions satisfying all boundary conditions, and each of them describes a deflection

of the entire system. For the  $i$ th span, the shape of the span deflection is superposed by sinusoidal waves  $\sin(k\pi x)$  for  $k = 1, \dots, N_i$ . For instance,  $\boldsymbol{\psi}_k = \{\sin k\pi x, 0, 0, 0, 0, 0, 0\}^T$  for the first span with  $k = 1, \dots, N_1$ . For the discrete pulleys and tensioner arm, the global comparison function involves only the relevant discrete element, such as  $\boldsymbol{\psi}_{p+2} = \{0, 0, 0, 0, 1, 0, 0\}^T$  for pulley 2. Using the inner product defined in reference [9], the discretized formulation is

$$[\mathbf{M}]\ddot{\mathbf{A}} + [\mathbf{G}]\dot{\mathbf{A}} + [\mathbf{K}]\mathbf{A} = \mathbf{F} \quad (7)$$

where  $\mathbf{A}(t) = \{a_1(t) \dots a_p(t) \theta_1 \theta_2 \theta_3 \theta_t\}^T$  are generalized coordinates.

In vehicles, the alternating engine cylinder ignition and compression strokes cause cyclic fluctuations of the crankshaft speed. One specifies the periodic speed irregularity  $\theta_1$  based on engine properties. For such specified crankshaft speed, the applied torque  $M_1$  on the driving pulley is omitted and all terms with  $\theta_1$  in equation (7) are moved to the right-hand side as excitation, which yields

$$\begin{aligned} \mathbf{M}^0 \ddot{\mathbf{A}}^0 + (\mathbf{G}^0 + \mathbf{C}^0) \dot{\mathbf{A}}^0 + \mathbf{K}^0 \mathbf{A}^0 &= \mathbf{f} \\ \mathbf{f} &= \mathbf{F}^0 - \begin{pmatrix} \vdots \\ [M]_{i,p+1} \ddot{\theta}_1 + [G]_{i,p+1} \dot{\theta}_1 + [K]_{i,p+1} \theta_1 \\ \vdots \end{pmatrix}, \\ i &= 1, \dots, p+4, \quad i \neq p+1 \end{aligned} \quad (8)$$

where the superscript 0 denotes the new matrices and vectors induced by the elimination of the  $(p+1)$ th row and column from the original ones.  $\mathbf{C}^0$  is a damping matrix obtained from modal damping to capture the energy dissipation in spans and bearings. The combination of (8) and (5) and the switching criteria in Table 1 fully describe the dynamic motion of the system.

### 3 METHODS

The system response for either engaged or disengaged clutch status can be found from the linear system theory. To decouple the equations in (8), a state-space variable  $\mathbf{z} = \{\mathbf{A}^0, \dot{\mathbf{A}}^0\}^T$  is introduced and equation (8) is transformed into

$$\begin{aligned} \dot{\mathbf{z}} &= \mathbf{R}\mathbf{z} + \mathbf{f}_F \\ \mathbf{R} &= \begin{bmatrix} \mathbf{0} & \mathbf{I} \\ -(\mathbf{M}^0)^{-1}\mathbf{K}^0 & -(\mathbf{M}^0)^{-1}(\mathbf{G}^0 + \mathbf{C}^0) \end{bmatrix}, \quad \mathbf{f}_F = \{\mathbf{0} \ \mathbf{f}\}^T \end{aligned} \quad (9)$$

where  $\mathbf{I}$  is a  $(p+3) \times (p+3)$  identity matrix. Furthermore, one finds the modal matrix  $\mathbf{V}$  of  $\mathbf{R}$  and introduces the modal coordinate vector  $\mathbf{q}$  as

$$\mathbf{z} = \mathbf{V}\mathbf{q} \quad (10)$$

Substituting equation (10) into equation (9) and left-multiplying  $\mathbf{V}^{-1}$  yield the decoupled equation

$$\dot{\mathbf{q}} = \boldsymbol{\Lambda}\mathbf{q} + \mathbf{h}, \quad \boldsymbol{\Lambda} = \mathbf{V}^{-1}\mathbf{R}\mathbf{V}, \quad \mathbf{h} = \mathbf{V}^{-1}\mathbf{f}_F \quad (11)$$

where  $\boldsymbol{\Lambda}$  is diagonal. The solution of equation (11) is

$$\mathbf{q}(t) = e^{\boldsymbol{\Lambda}t}\mathbf{q}(t_0) + \int_{t_0}^t e^{\boldsymbol{\Lambda}(t-\tau)}\mathbf{h}(\tau) d\tau \quad (12)$$

where  $t_0$  is the initial time and  $e^{\boldsymbol{\Lambda}(t-\tau)}$  is the transition matrix.

One can numerically evaluate the integral in equation (12). At any time instant  $t$ , however, the transition matrix has to be evaluated from  $t_0$  to  $t$  for integration. For numerical efficiency, one can save the transition matrix at each time instant  $t \in [t_0, t_f]$  to avoid repetitive matrix evaluation, where  $t_f$  is the final time. This works well for systems with few DOFs and few integration time points. For the current system and practical ones having more spans and pulleys, the discretized system has many DOFs and many oscillation cycles are required to ensure the complete decay of the transient response to capture the steady state. Therefore, numerical evaluation of equation (12) is inefficient.

Meirovitch [17] presents an analytical approximation in discrete time series that evaluates the solution at  $t_0, \dots, t_k, \dots, t_N$  for  $t_k = t_0 + k\Delta t$ , where  $N = (t_f - t_0)/\Delta t$ . This approximation is adopted herein as

$$\begin{aligned} \mathbf{q}(t_{k+1}) &= \boldsymbol{\Phi}\mathbf{q}(t_k) + \boldsymbol{\Gamma}\mathbf{f}_F(t_k), \quad k = 0, 1, \dots, N \\ \boldsymbol{\Phi} &= e^{\boldsymbol{\Lambda}\Delta t}, \quad \boldsymbol{\Gamma} = \boldsymbol{\Lambda}^{-1}(\boldsymbol{\Phi} - \mathbf{I})\mathbf{V}^{-1} \end{aligned} \quad (13)$$

where  $\Delta t$  is the sampling period chosen sufficiently small such that the input vector  $\mathbf{f}_F(t)$  can be regarded as constant over the time interval  $t_k < t < t_{k+1}$ . The use of equation (10) generates the physical response. The solutions are confirmed by numerical integration. This method requires 30–50 per cent of the computational time when compared with numerical integration.

The transition time instants for switching between the different clutch configurations must be determined. During engagement, the clutch torque is monitored. At each time instant, by obtaining the response from equations (13) and (10), the response

of the accessory  $\dot{\theta}_a$  and  $\ddot{\theta}_a$  is known because the accessory is moving together with the pulley. Hence, the clutch torque from equation (5) can be determined. If  $M_c = 0$  (or less than a specified tolerance in the numerical implementation), disengagement starts from the next time instant. In contrast, although the clutch is disengaged, the relative velocity is monitored.  $\dot{\theta}_p$  is obtained from equations (13) and (10), and  $\dot{\theta}_a$  is yielded from equation (5) with  $M_c = 0$ . If  $\dot{\theta}_p - \dot{\theta}_a = 0$  (within a specified tolerance), the clutch returns to engagement.

The above-mentioned method allows for unlimited switches between engagement and disengagement in a single cycle, unlike the analytical solution in reference [14], where only a single transition is assumed.

#### 4 RESULTS AND DISCUSSIONS

The steady-state periodic response of the system subjected to excitation from crankshaft speed fluctuation specified as  $\dot{\theta}_1 = D \cos \Omega t$  is considered. The excitation frequency  $\Omega$  is  $\sigma$  times the engine (crankshaft) speed, where  $\sigma$  is determined by the number of engine cylinders and  $\sigma = 3$  is used in the present work. The belt translation speed varies with the engine speed as  $s = r_1 \Omega / (\sigma l)$ . The range  $\Omega = 0-12$  corresponds to the engine speed varying over 0-5850 r/min for the parameters in Table 2, which is a frequency range of practical importance. The belt speed  $s = 0.921$  corresponding to  $\Omega = 12$  is lower than any critical speed that results in unstable operation of this gyroscopic system. The amplitude of the crankshaft speed fluctuation  $D$  is typically an estimated percentage  $\mu$  of the engine speed, thus  $D = \mu \Omega / \sigma$ . The value  $\mu = 10$  per cent is chosen, although this depends on engine speed in practice.

The parameter  $\alpha$  is the inertia ratio of the accessory and the driven pulley, i.e.  $m_a = \alpha m_p$ . Throughout the article, the combined inertia of the pulley and accessory is unchanged as  $m_0 = 26.03$  ( $J_0 = 0.01 \text{ kg m}^2$ ) for any  $\alpha$ . For the discretization,  $N_i = 2$  is chosen for  $i = 1, 2, 3$ , i.e. the half-sine and sine waves are considered. The modal damping coefficient to obtain

$C^0$  in equation (8) is  $\zeta = 5$  per cent and the accessory damping is  $c_g = 0.2$ .

As the excitation frequency  $\Omega$  varies, the belt speed and the eigensolutions of the linear system change [9]. For small bending stiffness, the natural frequencies of transversely dominant vibration modes decrease quickly with increasing speed, whereas those of rotationally dominant vibration modes change slightly. For large bending stiffness, all natural frequencies decrease comparably slowly and non-monotonically with speed because of the strong belt-pulley coupling. A moderate bending stiffness  $\varepsilon = 0.02$  is used in the present work. Simulations with different bending stiffnesses confirm that the major conclusions do not change from those obtained from this moderate value.

Two linear systems are considered for comparison with the non-linear system with the one-way clutch. One such system corresponds to the permanently engaged clutch case. This is called the 'locked clutch' system. It represents the standard arrangement in practical systems where there is no clutch and the pulley and accessory are rigidly connected. In this case,  $m_3 = m_0$ . The other system refers to the case when the clutch fully disengages and the belt only drives the pulley with inertia  $m_3 = m_p = m_0 / (1 + \alpha)$ . This is called the 'disengaged clutch' system.

The active driven inertia changes from the combined inertia (when the clutch is locked) to the pulley inertia (when the clutch is disengaged), and the natural frequencies vary accordingly. Figure 2 generated for belt speed  $s = 0.069$  ( $\Omega = 0.9$ ) illustrates this variation, where  $\alpha = 0$  corresponds to the natural frequencies of the locked clutch system. For the parameters in Table 2, the rotationally dominant modes have the lowest natural frequencies for both linear systems. According to Fig. 2,  $\Omega_1$  initially increases quickly with  $\alpha$ , but further increase of  $\Omega_1$  is indistinguishable for large  $\alpha$  and the tensioner arm eventually dominates this mode.  $\alpha$  does not impact the  $\Omega_2$  mode dominated by span transverse vibration. The accessory-pulley-dominant mode natural frequency, denoted by an  $x$  at  $\alpha = 0$ , increases monotonically with  $\alpha$ . For example,  $\Omega = 2.7$  when  $\alpha = 0$ ,

**Table 2** Physical properties of the example system

Pulley radius $r_1$	0.081 25 m	Pulley centre $(x_1, y_1)$	(0.5514, 0.0556) m
Pulley radius $r_2$	0.031 15 m	Pulley centre $(x_2, y_2)$	(0.3601, 0.0572) m
Pulley radius $r_3$	0.03 m	Pulley centre $(x_3, y_3)$	(0, 0)
Tensioner arm $r_t$	0.04 m	Pulley centre $(x_t, y_t)$	(0.3082, 0.0635) m
Rotational inertia $J_1$	0.072 48 kg m <sup>2</sup>	Belt modulus EA	120 000 N
Rotational inertia $J_2$	0.000 293 kg m <sup>2</sup>	Initial tension $P_0$	300 N
Rotational inertia $J_0$	0.01 kg m <sup>2</sup>	Belt mass density $\rho$	0.1029 kg/m
Rotational inertia $J_t$	0.001 165 kg m <sup>2</sup>	Tensioner stiffness $k_t$	28.25 N m/rad
Span length $l_1$	0.1548 m	Alignment angle $\beta_1$	135.79°
Span length $l_2$	0.3477 m	Alignment angle $\beta_2$	178.74°
Span length $l_3$	0.5518 m	Tensioner rotation $\theta_{tr}$	0.1688 rad
Damping ratio $\zeta$	5%		

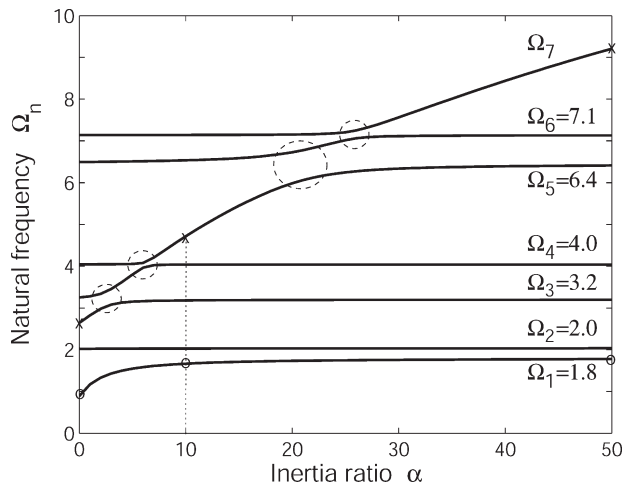


**Fig. 2** Natural frequencies of the disengaged clutch system varying with inertia ratio  $\alpha$  for belt speed  $s = 0.069$  ( $\Omega = 0.9$ ) and other parameters in Table 2. Dashed circles indicate regions of natural frequency veering

whereas  $\Omega = 4.7$  for  $\alpha = 10$  and  $\Omega = 9.2$  for  $\alpha = 50$ . Natural frequency veering occurs when the natural frequency of this mode approaches other natural frequencies. For instance, it approaches  $\Omega_3$ ,  $\Omega_4$ ,  $\Omega_5$ , and  $\Omega_6$  near  $\alpha = 2.7$ ,  $5.3$ ,  $21$ , and  $26$ , respectively (indicated in dashed circles in Fig. 2). Away from the veering zones, the modal properties remain the same for this mode, except that its natural frequency varies. The modal energy distributions of other modes and their associated natural frequencies approach steady configurations for large  $\alpha$ . The modes with  $\Omega_3$ – $\Omega_6$  for large  $\alpha$  are dominated by span transverse vibration. Figure 2 gives the limiting value of each natural frequency. These natural frequencies vary slightly when the belt speed (excitation frequency) changes.

#### 4.1 Excitation frequency sweep

Figure 3 gives the r.m.s. dynamic deflections of the half-sine wave of three spans ( $a_1$ ,  $a_3$ , and  $a_5$ ) and that of the sine wave of the second span ( $a_4$ ). The locked clutch system (representing the conventional pulley arrangement) and the disengaged clutch system for  $\alpha = 10$  are compared with the non-linear system. The common resonances occur in the transversely dominant modes, such as those at  $\Omega = 6.4$  of the first span (Fig. 3(a)),  $\Omega = 3.2$  and  $7.1$  of the second span (Figs 3(b) and (d)), and  $\Omega = 2.0$  of the third span (Fig. 3(c)). For excitation frequencies near these modes, the responses of the two linear systems bound the non-linear system response and determine the effectiveness of the vibration suppression by the one-way clutch, provided super-

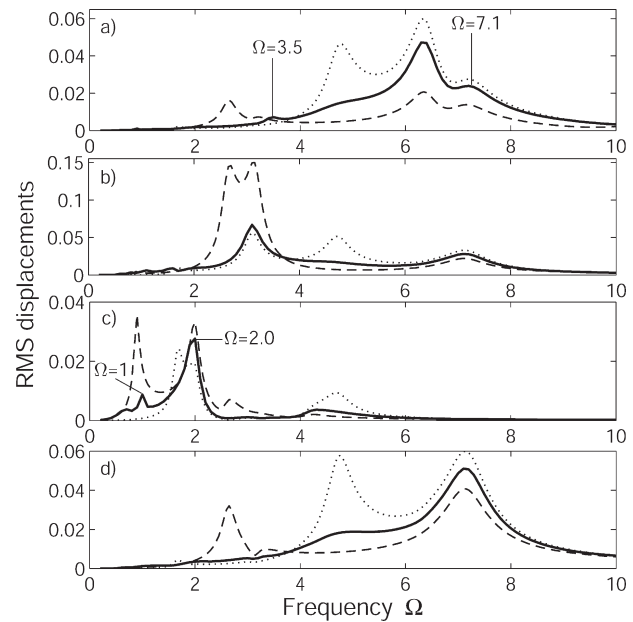


**Fig. 3** r.m.s. dynamic response of the deflection amplitudes for  $M_1 = 0.556$  and other parameters in Table 2. (a)  $a_1 - a_{1\text{mean}}$ ; (b)  $a_3 - a_{3\text{mean}}$ ; (c)  $a_5 - a_{5\text{mean}}$ ; and (d)  $a_4 - a_{4\text{mean}}$ . - - locked linear; ..... disengaged linear  $\alpha = 10$ ; — non-linear  $\alpha = 10$

sub-harmonic resonances do not occur. When the response of the locked clutch system is higher than that of the disengaged clutch case, the non-linear clutch suppresses the vibration, such as the modes at  $\Omega = 2.0$  in span 3 and  $\Omega = 3.2$  in span 2. In contrast, the vibration increases where the response of the disengaged clutch system is higher, such as the modes at  $\Omega = 6.4$  in span 1 and  $\Omega = 7.1$  in span 2.

Meanwhile, non-linear disengagement during part of a cycle strongly affects the rotationally dominant modes, such as those at  $\Omega = 0.9$  and  $2.7$  (Figs 3 and 4), where the resonances are markedly reduced in comparison with the locked clutch system. At frequencies where the disengaged clutch system has a natural frequency but the locked clutch system does not, such as  $\Omega = 4.7$ , the one-way clutch moves the locked clutch system towards the disengaged clutch one and the vibration increases.

Superharmonic resonances are evident in the span transverse vibrations in Fig. 3. Strong primary resonance occurs in span 3 near  $\Omega_2 = 2.0$  (Fig. 3(c)). One can see that a one-half-order non-linear superharmonic resonance of  $\Omega_2$  occurs at  $\Omega = 1.0$ , where the response frequency is  $\Omega = 2.0$ . Similarly, a one-half-order superharmonic of  $\Omega_6 = 7.1$  occurs near  $\Omega = 3.5$  in span 1 (Fig. 3(a)). Several other superharmonics with small amplitudes are associated with prominent resonances in each span. These secondary

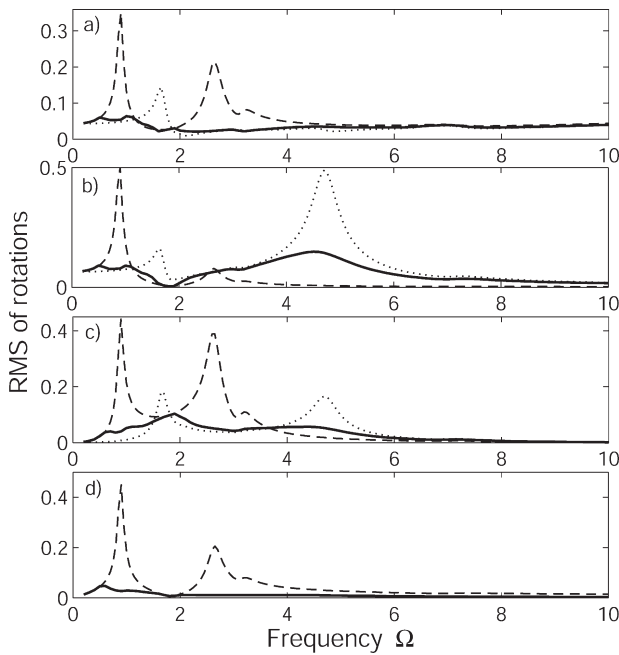


**Fig. 4** r.m.s. dynamic response of (a) tensioner pulley  $\theta_2 - \theta_{2\text{mean}}$ , (b) accessory pulley  $\theta_p - \theta_{p\text{mean}}$ , (c) tensioner arm  $\theta_t - \theta_{t\text{mean}}$ , and (d) accessory velocity  $\dot{\theta}_a - \dot{\theta}_{a\text{mean}}$  for  $M_1 = 0.556$  and other parameters in Table 2. -- locked linear; ..... disengaged linear  $\alpha = 10$ ; and — non-linear  $\alpha = 10$

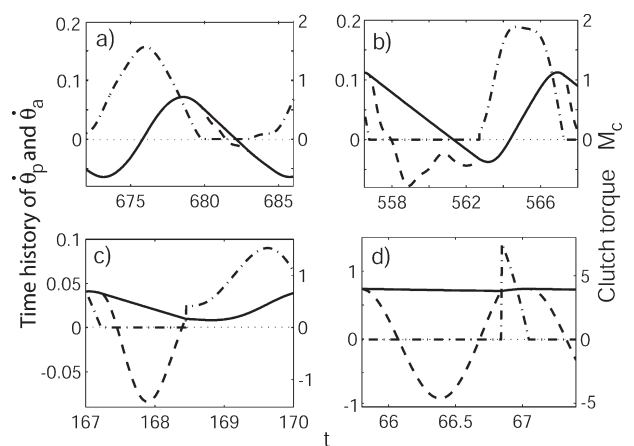
resonances have slight impact on system dynamics because of their small amplitudes.

The pulley and tensioner arm rotations are shown in Fig. 4. The accessory experiences zero-stiffness ‘free-wheeling’ without a steady mean during disengagement, so its rotational velocity, instead of rotation, is shown in Fig. 4(d). When the one-way clutch performs, the locked clutch resonance at  $\Omega = 0.9$  is removed. This shows the beneficial impact achievable with one-way clutches. The one-way clutch is so effective at this frequency, because the mode has a large accessory rotation. The non-linear system with  $\alpha = 10$  might be expected to show a corresponding increase at  $\Omega = 1.7$  because the disengaged system with  $\alpha = 10$  has a natural frequency there instead of  $\Omega = 0.9$  (Fig. 2). No such increase is evident. Similar behaviour showing the one-way clutch’s effectiveness is evident near the locked clutch resonance at  $\Omega = 2.7$ . For  $\alpha = 10$ , the corresponding natural frequency of the disengaged clutch system is at  $\Omega = 4.7$  after allowing for veering (Fig. 2). In this case, the non-linear system with  $\alpha = 10$  shows slightly elevated response at  $\Omega = 4.7$  (as might be expected because of the resonance introduced there by  $\alpha = 10$ ), but this increase is minor when compared with the benefit of the reduction at  $\Omega = 2.7$ . By selecting a sufficiently large

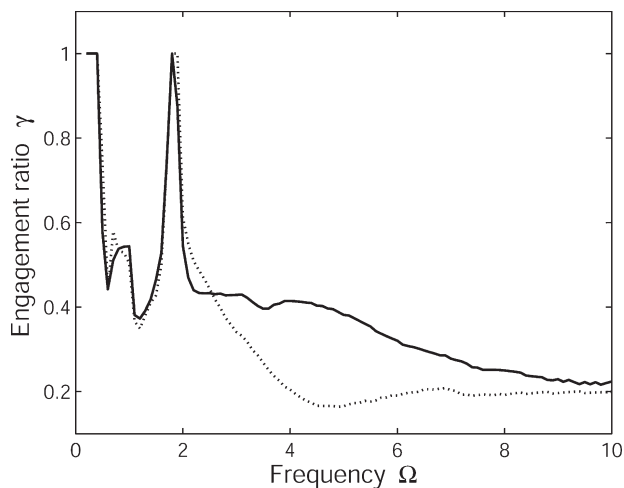
$\alpha$ , such as  $\alpha > 118$ , one can avoid the disengaged clutch resonances dominated by the accessory-pulley in the practically important frequency range  $\Omega = 0-12$ , and therefore no such increased rotational vibration occurs. In practice, limitations on available ranges of  $\alpha$  will require one-way clutch design to address particular speed ranges rather than all engine speeds. Regarding the accessory (Fig. 4(d)), the clutch isolates it during disengagement, suppressing the modal resonances of the locked clutch system dominated by rotational vibration such as those at  $\Omega = 0.9$  and  $2.7$ . This isolation and suppression are the reasons why one-way clutches are so effective.

Figure 5 shows the periodic velocity time histories of the driven pulley and accessory and the associated clutch torque at different frequencies. Disengagements occur in the deceleration phase to decouple the motions of the pulley and accessory. This removes the impact of the large accessory inertia on the pulley during deceleration. When there is small disengagement, both velocities have a sinusoidal-like profile. For  $\Omega = 0.5$ , the clutch disengages in a small portion of the cycle. For  $\Omega = 0.6$ , the disengagement expands and higher harmonics of the excitation frequency  $2\Omega$ ,  $3\Omega$ , and so on, are clearly evident in the velocity spectra. Figure 5(c), for  $\Omega = 2.0$ , shows a general case where the clutch torque jumps from zero for disengagement to non-zero as engagement begins. Similar but sharper behaviour occurs for  $\Omega = 5.0$  (Fig. 5(d)), where disengagement occurs over the majority of a cycle.

To track the engagement and disengagement behaviour of the clutch, an engagement ratio  $\gamma$  is introduced to quantify the percentage of a cycle for



**Fig. 5** Time history of the rotational velocities of the accessory pulley and accessory, and the associated clutch torque for  $\alpha = 10$ ,  $M_1 = 0.556$ , and other parameters in Table 2. (a)  $\Omega = 0.5$ ; (b)  $\Omega = 0.6$ ; (c)  $\Omega = 2.0$ ; and (d)  $\Omega = 5.0$ . —  $\dot{\theta}_a$ , --  $\dot{\theta}_p$ , and -.-  $M_c$



**Fig. 6** Engagement ratio varies with excitation frequency for  $M_1 = 0.556$  and other parameters in Table 2. ....  $\alpha = 10$  and —  $\alpha = 50$

which the clutch is engaged. Figure 6 shows the engagement ratio across the practically important frequency range for  $\alpha = 10$  and 50 and other parameters in Table 2. At low frequencies  $\Omega < 0.5$ , disengagement does not occur because the deceleration is mild. The deceleration is higher at high frequencies, which leads to more disengagement. The exception at  $\Omega = 1.8$ , where no disengagement occurs, results because the engaged system naturally has a very small response (and acceleration/deceleration) at that frequency. The one-way clutch is not called on to reduce vibration, so no disengagement occurs. For a given  $\alpha$ , more disengagement occurs near modal resonances of the disengaged clutch system dominated by the accessory-pulley such as  $\Omega = 4.7$  for  $\alpha = 10$ .

#### 4.2 Impact of inertia ratio

For  $\alpha \approx 1$ , the inertias of the pulley and accessory are similar. In this case, accessory disengagement with the pulley strongly impacts component response. On the contrary,  $\alpha \gg 1$  means that a small pulley drives a large accessory. Disengagements reduce the impact of the accessory on the system dynamics. For large enough  $\alpha$  ( $\alpha \approx 40$  here), further increases of the accessory inertia have minor effect because, other than the mode dominated by the accessory-pulley, the modes of the disengaged clutch system change only slightly (Fig. 2).

Figure 7 depicts how the engagement ratio  $\gamma$  varies with  $\alpha$ . For varying  $\alpha$ , if an excitation frequency  $\Omega$  induces resonance in either limiting linear system, the disengagement intensifies. For example,  $\Omega = 0.9$  is near the first-mode resonance of the locked

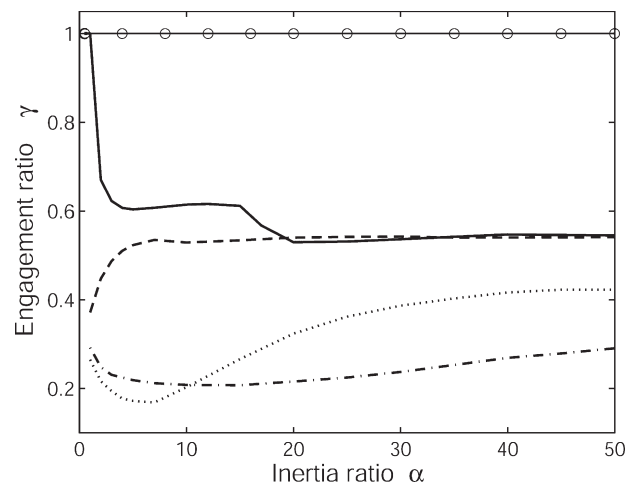


**Fig. 7** Engagement ratio varies with inertia ratio for  $M_1 = 0.556$  and other parameters in Table 2. --  $\Omega = 0.9$ ; —○—  $\Omega = 1.8$ ; —  $\Omega = 2.0$ ; ....  $\Omega = 4.2$ ; and -.-.  $\Omega = 7.1$

clutch system dominated by the accessory-pulley, and the rapid deceleration of the driven pulley and accessory at resonance introduces large clutch disengagement. For small, non-zero inertia ratio, there remains a near-resonant excitation frequency  $\Omega = 0.9$ , but the mode is that of the disengaged clutch system. In this case, the high response of the pulley further enlarges the disengagement. For further increase in  $\alpha$ ,  $\Omega = 0.9$  deviates away from the disengaged clutch resonance and the disengagement reduces.  $\Omega = 4.2$  is resonant during disengagement at  $\alpha = 7$ , where Fig. 7 shows the clutch to be most active and considerable disengagement occurs.  $\Omega = 7.1$  is near one of the natural frequencies of both linear systems across the inertia ratio range, and the response is large in both clutch configuration phases. Hence, the disengagement is large. Under the chosen external load  $M_1 = 0.556$ ,  $\Omega = 1.8$  does not introduce disengagement for any  $\alpha$ . The locked clutch system performs as desired (small vibration), and no clutch action takes place. For lower load values, disengagement could occur at  $\Omega = 1.8$ .

For all inertia ratios, the dynamic response of the accessory velocity is always lower than that of the locked clutch case  $\alpha = 0$  (Fig. 8(a)), and so the accessory benefits appreciably from the one-way clutch. The pulley response, however, which is an important practical consideration (for dynamic tension fluctuations and belt-pulley friction noise, for example), does not decrease monotonically (Fig. 8(b)).

#### 4.3 Impact of external load

During disengagement, the velocity of the accessory-pulley quickly re-approaches that of the accessory

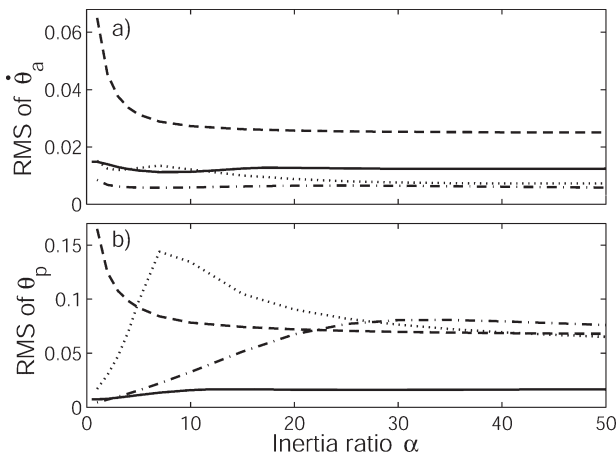


**Fig. 8** r.m.s. dynamic responses of (a) the accessory velocity and (b) the accessory pulley vary with inertia ratio for  $M_1 = 0.556$  and other parameters in Table 2. - -  $\Omega = 0.9$ ; —  $\Omega = 2.0$ ; ...  $\Omega = 4.2$ ; and - · -  $\Omega = 7.1$

when the accessory experiences a rapid deceleration from a large external load. Therefore, a higher load reduces disengagement, and a sufficient load can eliminate disengagement and the function of the one-way clutch. A lower load results in more disengagement.

Figure 9 shows the engagement ratio varying with load for different frequencies and  $\alpha = 50$ . The engagement increases with increasing load until the disengagement completely vanishes. The frequency branches  $\Omega = 0.9, 1.8, 2.0, 2.7,$  and  $7.1$  have critical loads for a locked clutch ( $\gamma = 1$ ) at  $M_1^{cr} \approx 15.1, 0.5, 1.0, 19.5,$  and  $5.0,$  respectively. The large critical loads for  $\Omega = 0.9$  and  $2.7$  are because these

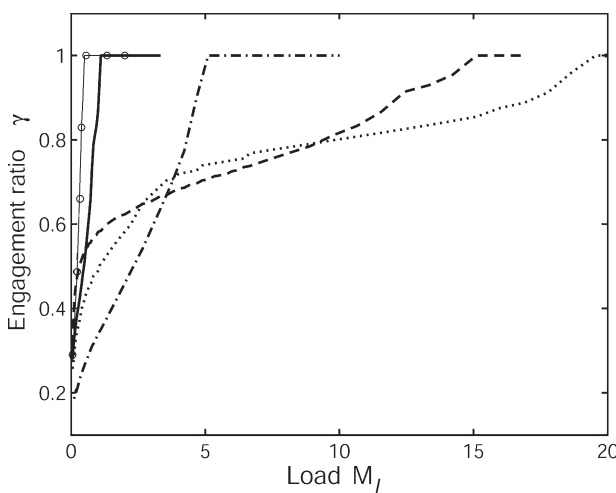


**Fig. 9** Engagement ratio varies with external load for  $\alpha = 50$  and other parameters in Table 2. - -  $\Omega = 0.9$ ; —○—  $\Omega = 1.8$ ; —  $\Omega = 2.0$ ; ...  $\Omega = 2.7$ ; and - · -  $\Omega = 7.1$

frequencies are near resonances of the locked clutch system ( $\alpha = 0$ ) dominated by pulley rotations.

The critical external load beyond which the system behaves with the locked clutch can be only obtained analytically. For the locked clutch limit, the accessory response  $\theta_a = B \sin(\Omega t + \vartheta)$  is sinusoidal, where  $B$  is determined from the analytical r.m.s. solution of the locked clutch system. The expression for the clutch torque from equation (5) is expanded as

$$M_c = m_a \ddot{\theta}_a + c_g \dot{\theta}_a + M_1 = B \sqrt{(m_a \Omega)^2 + c_g^2} \sin(\Omega t + \vartheta + \varphi) + M_1 \quad (14)$$

where  $\varphi = \tan^{-1}(c_g / (m_a \Omega))$ . The condition  $M_c = 0$  delineates the locked case from the non-linear one with disengagement, so the lowest external load  $M_1^{cr}$  that leads to a locked clutch for given frequencies is

$$M_1^{cr} = B \sqrt{(m_a \Omega)^2 + c_g^2} \quad (15)$$

To promote effective operation of the one-way clutch (i.e. disengagement), a load satisfying  $M_1 < M_1^{cr}$  is desirable; otherwise, the two components remain locked for the entire cycle.

Figure 10 shows two curves generated from equation (15) for varying excitation frequency. The critical load is large at the locked clutch resonances where the modal amplitude of the accessory is large, such as at  $\Omega = 0.9$  and  $2.7$ . At these frequencies, the one-way clutch is active and disengagements occur even for large loads (i.e.  $M_1 < M_1^{cr}$ ). Equation (15) indicates that the critical load depends on the inertia of the accessory. One-way clutches are most effective when integrated with high inertia

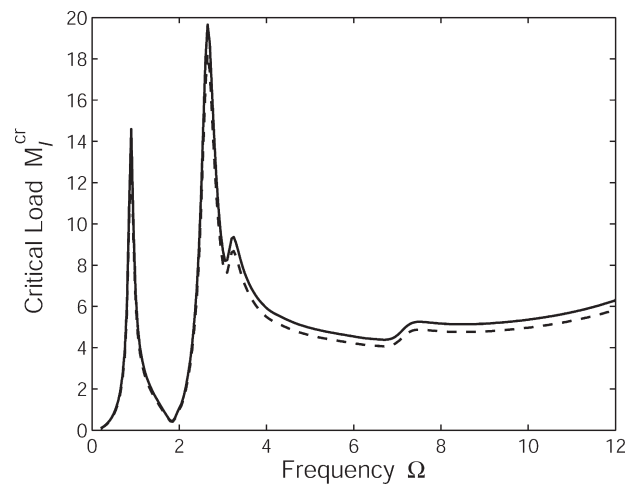


**Fig. 10** Critical external load varies across excitation frequency range for parameters in Table 2. - - -  $\alpha = 10$ ; and —  $\alpha = 50$

accessories, where they are also active across the widest range of accessory loads. From equation (15), they are also active for the greatest range of accessory loads at high excitation (i.e. engage) speeds.

**4.4 Impact on dynamic tension reduction**

Dynamic span tension amplitude is an important belt drive performance criterion. According to reference [9], the linearized dynamic tension of each span relative to the system without the steady accessory torque  $M_1$  is

$$\begin{aligned}
 P_{d1} &= \eta \left( -\frac{r_2}{l_1} \theta_2 + \frac{r_1}{l_1} \theta_1 - \frac{r_t}{l_1} \theta_t \sin \beta_1 + \int_0^1 w_{1,x} w_{1,x}^* dx \right) \\
 P_{d2} &= \eta \left( -\frac{r_3}{l_2} \theta_3 + \frac{r_2}{l_2} \theta_2 + \frac{r_t}{l_2} \theta_t \sin \beta_2 + \int_0^1 w_{2,x} w_{2,x}^* dx \right) \\
 P_{d3} &= \eta \left( -\frac{r_1}{l_3} \theta_1 + \frac{r_3}{l_3} \theta_3 + \int_0^1 w_{3,x} w_{3,x}^* dx \right)
 \end{aligned}
 \tag{16}$$

where the  $w_i^*(x)$  are equilibrium span deflections. The rotations of the pulleys and tensioner arm dominate the dynamic tensions in equation (16), where the integrals involving the span slopes are small.

Figure 11 exhibits the time history of the steady-state dynamic tension from equation (16) in a single cycle at  $\Omega = 2.0$ , in comparison with that of the locked clutch system. Dynamic tension is reduced in every span. The non-sinusoidal shapes of the dynamic tensions, especially shown in the second and third spans, reflect the alternate engagement

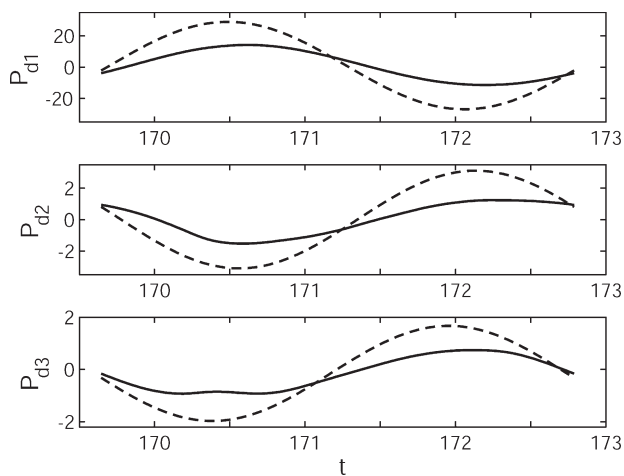


**Fig. 11** Time history of dynamic tensions of three spans for  $M_1 = 0.167$ ,  $\Omega = 2.0$ ,  $\alpha = 50$ , and other parameters in Table 2. — non-linear; and - - locked linear

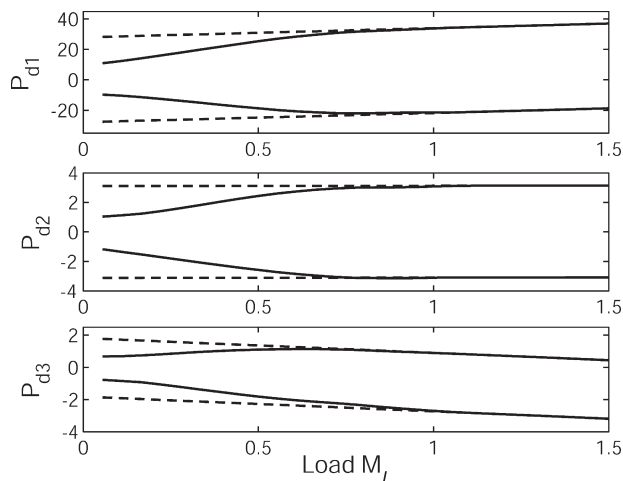


**Fig. 12** Maximum and minimum dynamic tensions of three spans vary with external load for  $\Omega = 2.0$ ,  $\alpha = 50$ , and other parameters in Table 2. — non-linear; and - - locked linear

and disengagement of the clutch. Figure 12 illustrates the maximum and minimum dynamic tensions varying with the external load, where the benefits of the one-way clutch are clearly evident at low loads. The tension drop induced by the one-way clutch decreases with increasing load until the tension curves merge with the linear ones because large load prevents disengagement. The maximum and minimum values of the non-linear system are not symmetric about the mean values of the linear dynamic tensions because of disengagement in part of a cycle.

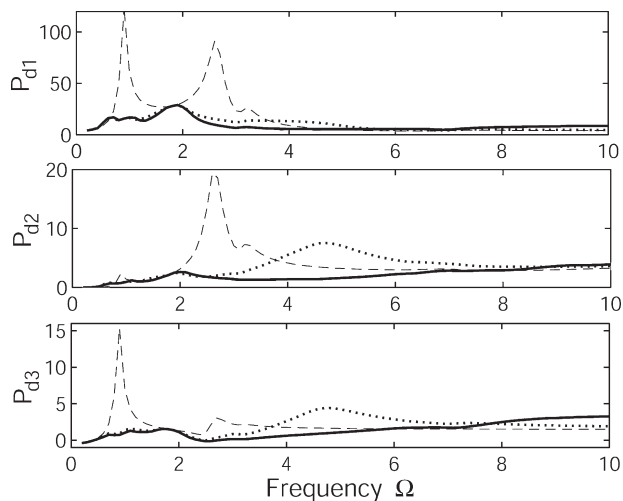


**Fig. 13** Maximum dynamic tensions of three spans vary across the frequency range for  $M_1 = 0.556$  and other parameters in Table 2. - - locked linear; — non-linear  $\alpha = 50$ ; and ... non-linear  $\alpha = 10$

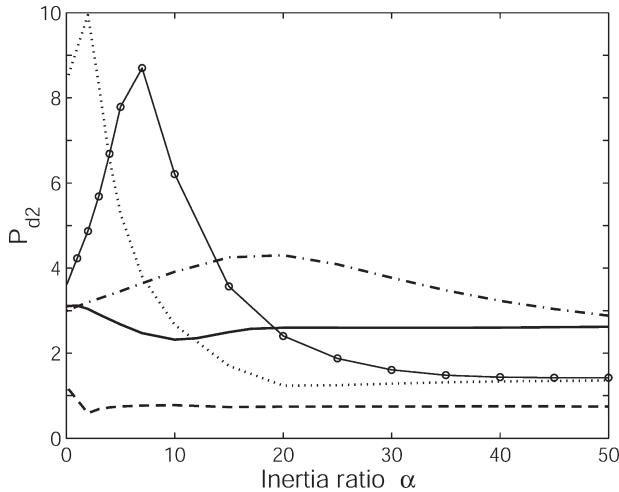


**Fig. 14** Maximum dynamic tension in span 2 varies with inertia ratio for  $M_1 = 0.556$  and other parameters in Table 2. --  $\Omega = 0.9$ ; —  $\Omega = 2.0$ ; ...  $\Omega = 3.2$ ; —○—  $\Omega = 4.2$ ; and -·-·  $\Omega = 7.1$

The maximum dynamic tensions varying with the excitation frequency are shown in Fig. 13, where they are compared with the locked clutch system. The rotations of the adjacent pulleys dominate the dynamic tension of each span. The pulley motion is the key factor. When a one-way clutch is present, the accessory motion plays no role during periods of disengagement. Consistent with Fig. 4, the dynamic tensions are significantly reduced because of the one-way action except at frequencies near the disengaged clutch resonances such as  $\Omega = 4$ . Figure 14 takes the second span as an example to illustrate the impact of the inertia ratio on the dynamic tension for a variety of frequencies. When a small pulley is associated with a big accessory ( $\alpha$  is large), significant disengagement occurs during a cycle, which releases the entire system from the accessory inertia and its load. As a result, lower dynamic tension results for large  $\alpha$  compared with the locked clutch case ( $\alpha = 0$ ).

### 5 SUMMARY AND CONCLUSIONS

The prototypical three-pulley serpentine drive with belt bending stiffness is extended with a one-way clutch that transmits power only in one direction and disengages the accessory when the pulley and accessory begin to move in opposite directions. This model leads to a piece-wise linear system, and the switching conditions are zero clutch torque and zero relative velocity for engagement and disengagement configurations, respectively. The transition matrix is used to evaluate the system response for each configuration using discrete time

series, which dramatically reduces computational time.

For the periodic excitation from the driving pulley, the steady-state periodic response is investigated across the practically important range of driving pulley (e.g. engine) excitation frequencies. The active pulley-accessory inertia changes when the clutch switches from engagement to disengagement. Natural frequencies vary accordingly.

Compared with the locked clutch system representing the typical belt drive arrangement, the rotational vibrations are noticeably suppressed, provided the frequency is away from the disengaged clutch natural frequencies whose modes are dominated by the accessory-pulley. This makes such natural frequencies important design considerations and key factors in establishing the speed/frequency ranges where the one-way clutch is most effective. The greatest vibration reduction, compared with the systems without a one-way clutch, occurs near resonances of modes dominated by the accessory-pulley.

For the span transverse vibration, non-linear superharmonic resonances occur that slightly increase the vibrations and dynamic tensions. Their impact is small when compared with the overall system vibration reduction. Not all span vibrations decrease as a result of the one-way clutch, however. The analysis of the disengaged clutch system (requiring only linear analysis) indicates which spans and excitation frequency ranges lead to higher response, compared with the conventional locked clutch case.

The inertia ratio  $\alpha$  reflecting the distribution of the fixed total inertia between the driven pulley and accessory significantly affects the dynamics. For large  $\alpha$  (i.e. large accessory inertia with small pulley), the disengaged clutch natural frequencies can possibly be pushed outside the operating frequency range, avoiding the negative performance impact from resonance at these frequencies. In practice, one will likely have to be satisfied to tune these frequencies to reduce the impact in the frequency ranges of most importance.

The one-way clutch is of greatest benefit for small accessory loads (torques). In this case, the accessory load does not decelerate the disengaged accessory as rapidly, so the disengagement that decouples the accessory inertia from the rest of the system has greater effect. An analytical estimate is determined for the critical accessory load above which the one-way clutch is inactive (i.e. the conventional configuration). This critical load increases with accessory inertia and excitation frequency.

The one-way clutch performance significantly reduces the dynamic span tensions, especially for low accessory loads, large accessory inertia, or near

resonant excitation frequency. The dynamic tension of the spans that are adjacent to the pulley integrated with the one-way clutch experience more impact from the clutch performance than other spans. Smaller external load admits more disengagement for a given frequency and thus more tension reduction.

#### ACKNOWLEDGEMENT

The authors are grateful to Mark IV Automotive/Dayco Corporation for their support and to Dr Linyuan Kong for help understanding his prior work.

#### REFERENCES

- 1 **Barker, C. R., Oliver, L. R., and Breig, W. F.** Dynamic analysis of belt drive tension forces during rapid engine acceleration. 1991 SAE International Congress and Exposition, Detroit, Michigan, 25 February–1 March 1991.
- 2 **Hwang, S.-J., Perkins, N. C., Ulsoy, A. G., and Meckstroth, R. J.** Rotational response and slip prediction of serpentine belt drive systems. *ASME J. Vibr. Acoust.*, 1994, **116**, 71–78.
- 3 **Leamy, M. J. and Perkins, N. C.** Nonlinear periodic response of engine accessory drives with dry friction tensioners. *ASME J. Vibr. Acoust.*, 1998, **120**, 909–916.
- 4 **Ulsoy, A. G., Whitesell, J. E., and Hooven, M. D.** Design of belt-tensioner systems for dynamic stability. *ASME J. Vibr. Acoust. Stress Reliab. Des.*, 1985, **107**, 282–290.
- 5 **Beikmann, R. S., Perkins, N. C., and Ulsoy, A. G.** Free vibration of serpentine belt drive systems. *ASME J. Vibr. Acoust.*, 1996, **118**, 406–413.
- 6 **Beikmann, R. S., Perkins, N. C., and Ulsoy, A. G.** Non-linear coupled vibration response of serpentine belt drive systems. *ASME J. Vibr. Acoust.*, 1996, **118**, 567–574.
- 7 **Zhang, L. and Zu, J. W.** Modal analysis of serpentine belt drive systems. *J. Sound Vibr.*, 1999, **222**(2), 259–279.
- 8 **Kong, L. and Parker, R. G.** Equilibrium and belt–pulley vibration coupling in serpentine belt drives. *ASME J. Appl. Mech.*, 2003, **70**, 739–750.
- 9 **Kong, L. and Parker, R. G.** Coupled belt–pulley vibration in serpentine drives with belt bending stiffness. *ASME J. Appl. Mech.*, 2004, **71**, 109–119.
- 10 **Vernay, P., Ferraris, G., Delbez, A., and Ouplomb, P.** Transient behaviour of a sprag-type over-running clutch: an experimental study. *J. Sound Vibr.*, 2001, **248**(3), 567–572.
- 11 **King, R. and Monahan, R.** Alternator pulley with integral overrunning clutch for reduction of belt noise. In 1999 SAE International Congress and Exposition, Detroit, Michigan, 1–4 March.
- 12 **Solfrank, P. and Kelm, P.** The dynamic simulation of automobile accessory drives. 1999, available from <http://www.ina.de>.
- 13 **Zhu, F. and Parker, R. G.** Nonlinear dynamics of a one-way clutch in belt–pulley systems. *J. Sound Vibr.*, 2005, **279**(1), 285–308.
- 14 **Mockensturm, E. M. and Balaji, R.** Piece-wise linear dynamic systems with one-way clutches. *ASME J. Vibr. Acoust.*, 2005, **127**(5), 475–482.
- 15 **Leamy, M. J. and Wasfy, T. M.** Transient and steady-state dynamic finite element modeling of belt-drives. *ASME J. Dyn. Syst. Meas. Control*, 2002, **124**, 575–581.
- 16 **Zhu, F. and Parker, R. G.** Perturbation analysis of a clearance-type nonlinear system. *J. Sound Vibr.*, 2006, **292**, 969–979.
- 17 **Meirovitch, L.** *Principles and techniques of vibrations*, 1997, p. 694 (Prentice-Hall, Inc., Upper Saddle River, New Jersey).